International Communications in Heat and Mass Transfer 177 (2026) 111437

Contents lists available at ScienceDirect

International Communications in Heat and Mass Transfer

journal homepage: www.elsevier.com/locate/ichmt

Hydrothermal assessment of a hybrid geometry-optimized microchannel and internal jet-impingement cooling architecture for advanced chips

Sultan Alshehery [a], Dan Dobrotă [b], Augustin Stoica [b], Hussain Sawwan [c], Salman Saeidlou [d], Nemat Mashoofi Maleki [e,*], Ibrahim Mahariq [f,g,h,i,j,*]

[a] Department of Mechanical Engineering, College of Engineering, King Khalid University, Abha, Saudi Arabia
[b] Faculty of Engineering, Lucian Blaga University of Sibiu, 550024 Sibiu, Romania
[c] Department of Chemical Engineering, College of Engineering, King Khalid University, Abha 61411, Saudi Arabia
[d] Sustainable Engineering and the Built Environment, School of Science, Psychology, Arts and Humanities, Computing, Engineering & Sport, Canterbury Christ Church University, Canterbury, Kent CT11QU, UK
[e] Department of Engineering, Khazar University, Baku, Azerbayjan
[f] College of Engineering and Architecture, Gulf University for Science and Technology, Mishref, Kuwait
[g] Department of Electrical and Electronic Engineering, Faculty of Engineering and Architecture, Istanbul Gelisim University, Avcılar- Istanbul, 34310, Istanbul, Türkiye
[h] Najjad Zeenni Faculty of Engineering, Al-Quds University, Jerusalem, Palestine
[i] Department of Medical Research, China Medical University Hospital, China Medical University, Taichung, Taiwan
[j] University College, Korea University, Seoul 02481, South Korea

ARTICLE INFO

Keywords:
Microchannel cold plate
Jet impingement cooling
Thermal-hydraulic performance
Thermal resistance
Energy reuse capability

ABSTRACT

The increasing power density of modern electronic chips demands advanced cooling solutions capable of high heat removal and temperature uniformity. This study experimentally investigates a hybrid cooling architecture integrating microchannel cold plates with internal jet impingement. In this design, water jets are delivered through small-nozzle tubes that are strategically distributed along the microchannel to provide localized heat-transfer enhancement. Three microchannel geometries—rectangular, arc-shaped, and sinusoidal—are evaluated under heat loads of 500–1000 W and flow rates of 1–4 *l*/min. Results indicate that the sinusoidal geometry achieves the highest overall hydrothermal efficiency, with jet integration yielding substantial performance gains. At 4 *l/min* and 1000 W, the hybrid sinusoidal design enhances the Nusselt number by 37.3% and reduces thermal resistance by 21.8%, while lowering the average surface temperature by up to 16 °C compared to a conventional plain cold plate. The thermal enhancement factor reaches 1.278, despite an associated pressure drop penalty. Furthermore, the hybrid design reduces the minimum flow rate required for safe operation and enhances energy reuse capability, achieving up to an 11% increase in the Energy Reuse Factor (ERF) compared to the traditional plain cooling block.

1. Introduction

The rapid growth of data-intensive technologies, including large-scale cloud computing, 5G communication networks, and modern AI workloads, has significantly increased the demand for high-performance CPUs and GPUs in data centers. These devices operate at power densities exceeding 1000 W/cm^2 in localized hotspots [1], imposing stringent thermal management requirements. If not effectively dissipated, such heat fluxes lead to rapid temperature rise, reduced reliability, shortened lifespan, and potential device failure. Conventional air-cooling has reached its practical limits and can no longer maintain safe junction temperatures in advanced electronic systems [2]. Consequently, liquid-based cooling approaches have gained increasing attention.

Liquid-cooling technologies are broadly classified into direct liquid cooling (DLC), where the coolant directly contacts the heat-generating surface (e.g., immersion [3] and spray cooling [4]), and indirect liquid cooling (ILC), in which heat is transferred through an intermediate solid interface, such as conventional cold plates (CPs), microchannel cold plates (MCH CPs) [5], and jet-impingement-based cold plates [6]. Among these, microchannel cold plates have emerged as a leading solution due to their compact structure, high heat removal capability, and cost-effective integration into electronic cooling systems. Enhancing their thermal–hydraulic performance requires continuous optimization

* Corresponding authors at: Department of Engineering, Bonab University, Bonab, Iran.
E-mail addresses: nemat.m.maleki@gmail.com (N.M. Maleki), ibmahariq@gmail.com (I. Mahariq).

https://doi.org/10.1016/j.icheatmasstransfer.2026.111437

Available online 11 May 2026

Nomenclature

Abbreviations

Symbol	Description
CP	Cold Plate
COP	Coefficient of Performance
CPU	Central Processing Unit
DLC	Direct Liquid Cooling
ERF	Energy Reuse Factor
GPU	Graphics Processing Unit
IGBT	Insulated Gate Bipolar Transistor
ILC	Indirect Liquid Cooling
JI	Jet Impingement
MCH CP	Microchannel Cold Plate
MJMC	Multi-Jet Microchannel
TDP	Thermal Design Power
TEF	Thermal Enhancement Factor

Symbols

A_c	Cross-sectional area of the microchannel (m^2)
C	Distribution coefficient for measurement error
C_p	Specific heat capacity of the working fluid (J/kg·K)
D_h	Hydraulic diameter of the microchannel (m)
f	Fanning friction factor
f_p	Fanning friction factor for the reference configuration (plain cold plate)
h	Convective heat transfer coefficient ($W/m^2 \cdot K$)
k	Thermal conductivity of the working fluid (W/m·K)
L	Length of the microchannel (m)
l	Wetted perimeter of the microchannel (m)
$\dot{m}$	Mass flow rate of the working fluid (kg/s)
Δm	Instrument accuracy
N_i	Individual measured value
$\bar{N}$	Arithmetic mean of measurements
n	Number of repeated trials
Nu	Nusselt number
Nu_0	Nusselt number for the reference configuration (plain cold plate)
P_i	Inlet pressure (Pa)
P_o	Outlet pressure (Pa)
Q	Heat transfer rate (W)
$Q_{captured}$	Captured thermal energy (W or J)
Re	Reynolds number
R_{th}	Thermal resistance (°C/W)
T_c	Condenser temperature (heat pump outlet) (K or °C)
T_{ev}	Evaporator temperature (microchannel outlet) (K or °C)
T_i	Inlet temperature of the working fluid (K or °C)
T_o	Outlet temperature of the working fluid (K or °C)
$T_{s,\ avg}$	Average surface temperature of the cold plate (K or °C)
$T_{s,\ 1-4}$	Individual thermocouple readings on the cold plate surface (K or °C)
$T_{w,\ avg}$	Mean fluid temperature (K or °C)
U	Overall measurement uncertainty
u_A	Type A uncertainty (statistical variation)
u_B	Type B uncertainty (systematic error)
u	Average velocity of the working fluid (m/s)
W	Width of the microchannel (m)
ΔT	Temperature difference used in thermal resistance calculation (K or °C)
η_{reuse}	Efficiency of the heat reuse process (e.g., COP)
μ	Dynamic viscosity of the working fluid (Pa·s)
ρ	Density of the working fluid (kg/m^3)

of microchannel geometry, including cross-sectional design, surface features, and flow-distribution pathways. In parallel, extensive studies have examined the effects of coolant type [7,8] and operating conditions, particularly inlet temperature and flow rate, on heat dissipation, underscoring the combined role of geometric design and operating parameters in performance optimization.

Jiahao Hu et al. [9] investigated microchannels incorporating topology-optimized ribs in straight, wavy, and fan-shaped configurations to enhance forced liquid cooling. Their simulations showed that, in wavy channels, the optimized rib design reduced the channel-base temperature by 71.4%, 30.1%, and 27.0% compared to configurations without ribs and with circular and square ribs, respectively. Overall, topology-optimized designs consistently improved both flow and thermal performance, with the wavy configuration achieving the highest effectiveness. Guangtao Zhai et al. [10] numerically investigated the thermal–hydraulic performance of honeycomb-structured microchannel cold plates for IGBT modules, examining the effects of cell size, channel spacing, inlet–outlet configuration, and operating conditions on peak temperature, temperature uniformity, and pressure loss. Results showed that an optimized honeycomb geometry reduces the maximum temperature. Multi-inlet–outlet configurations were found to reduce pressure loss and slightly enhance temperature uniformity, whereas increasing flow rate lowers peak temperature and improves uniformity at the expense of substantially higher pressure loss.

Liang Du et al. [11] numerically investigated the thermal–hydraulic performance of diamond microchannel heat sinks with various rib configurations, including rhombic transverse, orthogonal, and vertical arrangements, as well as various rib geometries, including square, triangular (forward and reverse), and circular geometries. Results showed that orthogonal ribs enhance fluid mixing in two directions and increase the solid–liquid contact area, leading to significant heat transfer enhancement, by 182.8% and 146.3% compared to transverse and vertical ribs, respectively, at the cost of increased pressure loss by 1000% and 17.5%. Wang and Tao [12] investigated the thermal performance of CPU cold plates by comparing *Z*-, I-, and U-type inlet/outlet manifolds and examining the effect of microchannel layer count on pressure loss and achievable CPU power. Results showed that the I-type configuration provides the most efficient flow and heat removal. Increasing the number of microchannel layers significantly reduces hydraulic losses, with the I-type-5 L design lowering pressure loss by 89.5% and increasing maximum CPU power by 22.9% compared to a single-layer plate.

Beyond microchannel configurations, whose compact geometry and high surface-area-to-volume ratio enable strong thermal performance, jet impingement (JI) cooling has attracted significant attention for its ability to provide intense localized heat removal. Elliott and Robinson [13] evaluated a jet-impingement-based cold plate for CPU cooling by varying the number of jets, jet diameter, spacing, and standoff distance, and assessed the resulting effects on junction temperature, pressure drop, pumping power, and core-to-coolant thermal resistance. They further compared single- and multi-objective optimization strategies. The single-objective design employed a limited number of high-velocity jets focused on the CPU core, reducing temperature by more than 10 K below the throttling threshold but requiring near-maximum pumping power. In contrast, the multi-objective design distributed numerous low-velocity jets over a wider area, increasing junction temperature by approximately 9 K while reducing pumping power.

Beyond standalone jet impingement, recent studies have increasingly explored hybrid architectures that combine jet impingement with microchannels or finned cold plates. Qidong Sun et al. [14] investigated

a hybrid microchannel–jet impingement cooling strategy for high heat flux applications, evaluating three inlet–outlet configurations over heat fluxes of 83–200 W/cm^2. All configurations demonstrated strong cooling capability; however, the 4IN5OUT layout exhibited the best thermo-hydraulic performance. At 200 W/cm^2, this design achieved an average surface temperature of 51 °C with a pressure loss of 31 kPa, while maintaining a peak temperature below 67.3 °C. Ming Peng et al. [15] investigated a multi-jet microchannel (MJMC) heat sink to examine how jet count, channel aspect ratio, fin-to-channel width ratio, and outlet width influence thermal–hydraulic performance. The MJMC design, integrating impinging jets with microchannel entrance effects, reduced pressure loss, lowered thermal resistance, and improved bottom-surface temperature uniformity compared to a conventional microchannel. Parametric analysis indicated that performance increases with more jets, a wider outlet, and a smaller fin-to-channel width ratio, while the aspect ratio exhibits an optimum near 6. M. Zunaid et al. [16] numerically studied a 45° inclined microjet-array heat sink for electronic cooling, examining the effects of jet count, diameter, and jet-to-surface distance on surface temperature, pressure loss, and temperature uniformity. Results showed that increasing the number of jets improved coolant distribution, enhanced vortex formation, and lowered surface temperature, while reducing pressure loss due to smaller flow per jet. Smaller jet diameters further reduced surface temperature but imposed a higher pressure penalty. W. Gao et al. [17] investigated a hybrid cooling configuration combining jet impingement with a trapezoidal-finned heat sink featuring secondary channels. Numerical simulations examined the impact of geometric parameters and jet-hole arrangements on heat transfer, pressure loss, and overall thermal performance. Results indicated that these design choices strongly influence the thermal–hydraulic response: unilateral jet patterns produced the highest heat-transfer coefficients, while bilateral arrangements offered a more balanced performance.

Given the critical role of thermal management in high-power electronic chips, microchannel cooling and jet impingement have emerged as two highly effective techniques, with their integration offering significant synergistic potential. In conventional designs, jet impingement is typically implemented externally, where the coolant is first distributed within an upper plenum and subsequently discharged through a nozzle plate above the cold plate surface. In contrast, this study introduces, for the first time, an internalized jet-impingement mechanism based on a branch-manifold structure embedded directly within the microchannel. This approach fundamentally alters flow distribution, jet formation, and boundary layer interaction compared to conventional configurations. Building on this concept, the study systematically evaluates both the standalone performance of the proposed architecture and its synergistic interaction with various microchannel geometries, including rectangular, arc-shaped, and sinusoidal designs, under identical operating conditions. Additionally, a structured methodology is developed to determine the minimum flow rate required to maintain safe operating temperatures. The performance assessment is further

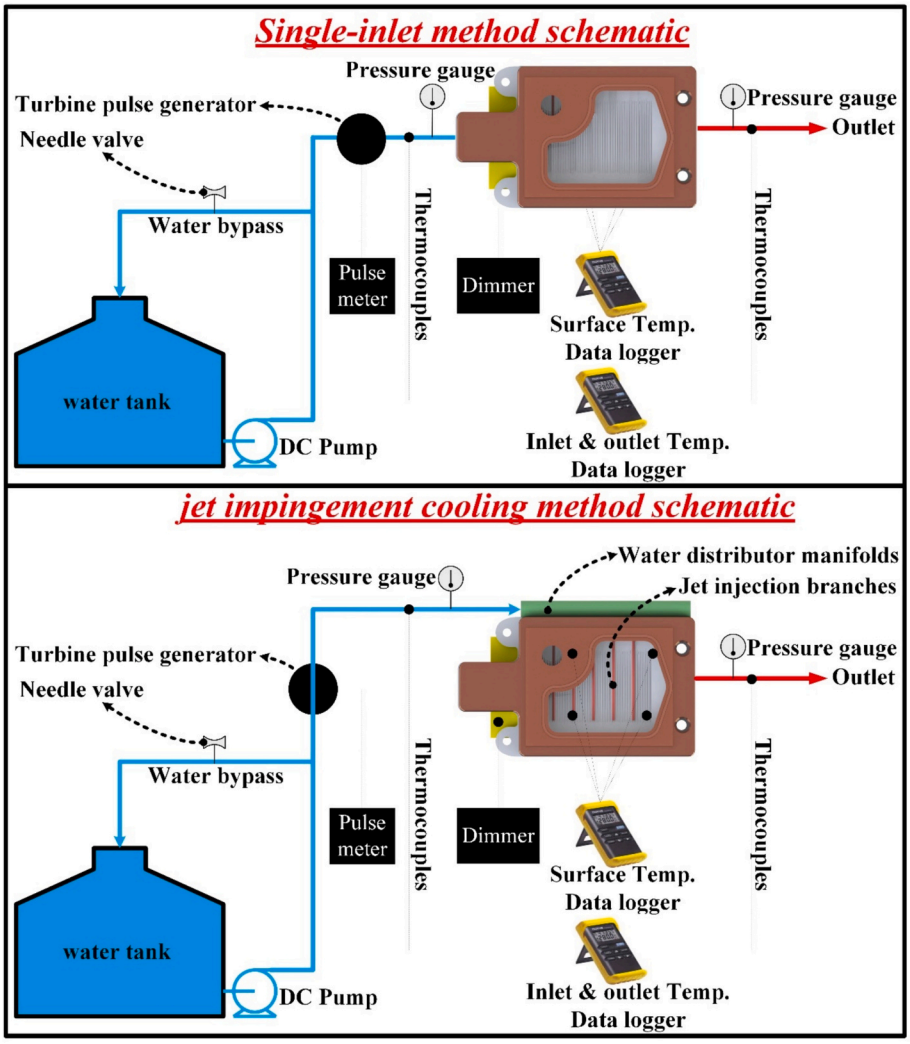

Fig. 1. Single-inlet method and jet impingement cooling method schematic.

extended beyond conventional thermo-hydraulic metrics by incorporating energy reuse capability through the Energy Reuse Factor (ERF).

2. Experimental setup and procedure

The experimental setup used in this study—designed to evaluate the influence of microchannel geometries and jet impingement cooling on key thermal and hydraulic parameters—is illustrated in Fig. 1. The system operates in an open-loop configuration and consists of a test section, water reservoir, centrifugal pump, turbine flowmeter, control valves, thermocouples, and a gauge pressure meter.

The working fluid, deionized water, is stored in the primary reservoir at 25 °C and delivered to the microchannel by the centrifugal pump. After passing through the pump and control valves, the flow rate is regulated by the turbine flowmeter and adjusted between 1 and 4 l/min, corresponding to Reynolds numbers of 1590 to 6370. Upon completing the heat-exchange process inside the microchannel, the fluid exits at an elevated temperature and is directed to a secondary reservoir. The inlet and outlet temperatures of the microchannel are monitored using type-K thermocouples connected to a dual-channel data logger. The cold plate surface temperature is recorded by four additional type-K thermocouples mounted on the plate and tracked with a separate data logger. The pressure drop across the microchannel is measured using a gauge pressure sensor. The tested microchannels have an effective area of 40 × 60

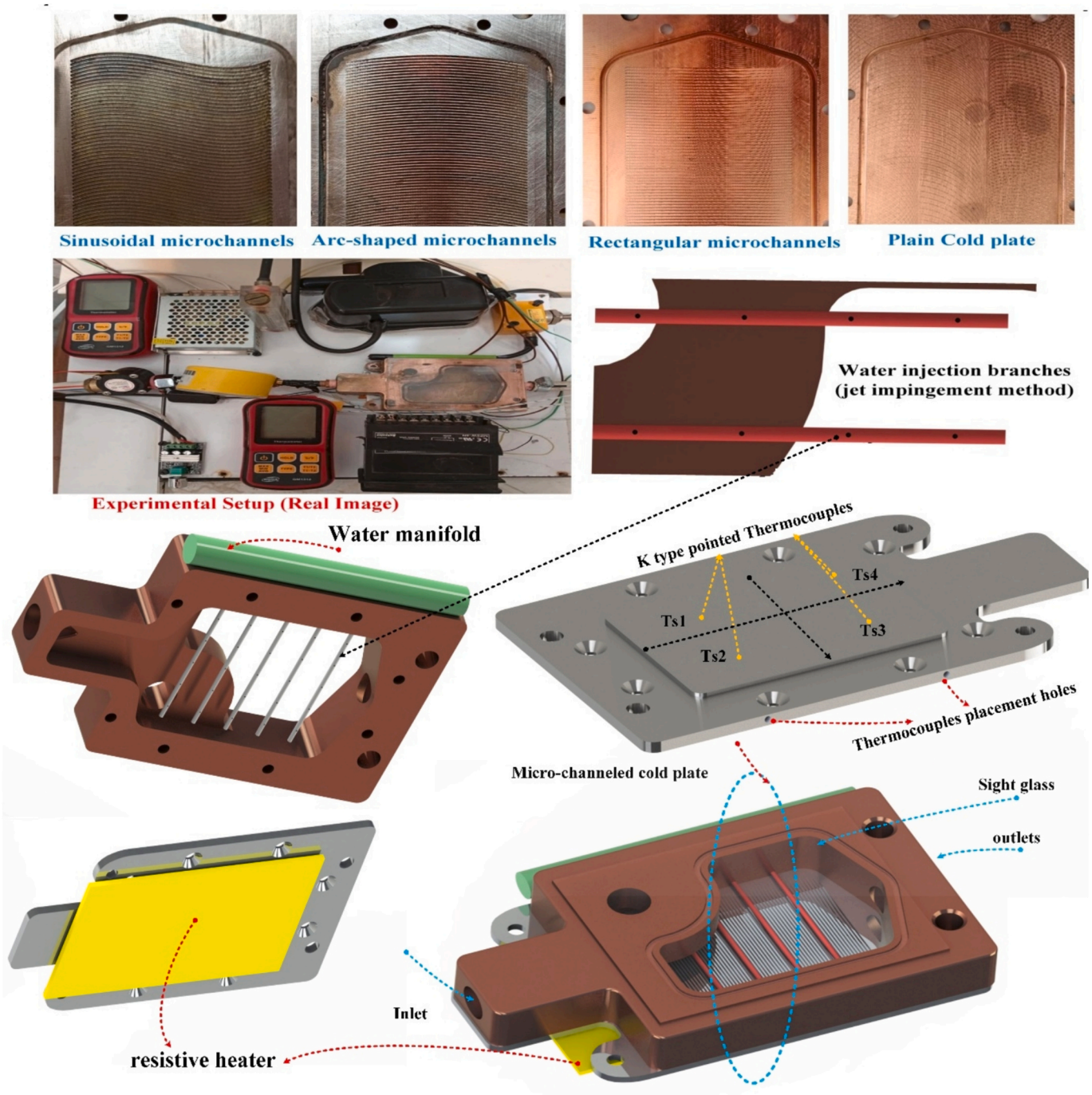

Fig. 2. Real image and schematic of the experimental setup and cooling block components, showing the locations of the four surface thermocouples (T_{s1}–T_{s4}) mounted inside the cold plate.

mm and comprise two main components: a microchannel cold plate and a cover plate. A resistive heating module is employed to apply a uniform heat flux to the underside of the cold plate, with the supplied heat load—referred to in this study as the thermal design power (TDP)—adjustable between 500 and 1000 W using a dimmer controller.

A resistive heating module is employed to apply a uniform heat flux to the underside of the cold plate. The module consists of four cartridge heaters (each rated at 300 W) embedded in an aluminum block (thermal conductivity ~205 W/m·K). The top surface of the aluminum block is precisely machined flat and coated with a thin layer of thermal interface material (thermal grease, 0.05 mm thickness) to minimize contact resistance with the cold plate. The supplied heat load—referred to in this study as the thermal design power (TDP)—is adjustable between 500 and 1000 W using a dimmer controller. Because the heat input is uniform and the cooling architectures are symmetrically arranged, the surface temperature distribution is expected to be reasonably uniform. Therefore, four surface thermocouples (T_{s1}–T_{s4} are mounted inside the cold plate as illustrated in Fig. 2), evenly distributed over the 40 × 60 mm area and aligned with the four primary heat-source zones of modern CPUs/GPUs, are sufficient to determine the average surface temperature with good fidelity. (See Fig. 3.)

Two independent flow-delivery mechanisms are evaluated for introducing the working fluid into the microchannel. In the first mechanism, referred to in this study as the single-inlet method, the fluid enters the microchannel through a single inlet at the upstream end and exits through a single outlet downstream. In the second mechanism, the fluid first enters a water-distributor manifold and is subsequently divided among five branches equipped with jet nozzles that are uniformly arranged along the microchannel with 10 mm intervals. In this configuration, the fluid is discharged directly onto the cold plate surface through high-velocity jet nozzles, thereby establishing jet impingement cooling. Each branch contains four jet nozzles with a diameter of 5 mm, resulting in a total of 20 nozzles across the microchannel.

The study is conducted in two main phases. The first phase focuses on independently assessing the effect of microchannel geometry on thermo-hydraulic performance. Four geometries—simple, rectangular, arc-shaped, and sinusoidal—are examined, and their performance is compared in terms of Nusselt number, friction factor, thermal resistance, cold plate surface temperature, and TEF. In this phase, fluid delivery follows the single-inlet method. In the second phase, the flow-delivery mechanism is modified, and all microchannel geometries are evaluated using the jet impingement configuration. Finally, the study identifies the minimum flow rate necessary to ensure a safe surface temperature for each configuration and assesses how microchannel geometry and operational conditions impact the energy reuse potential.

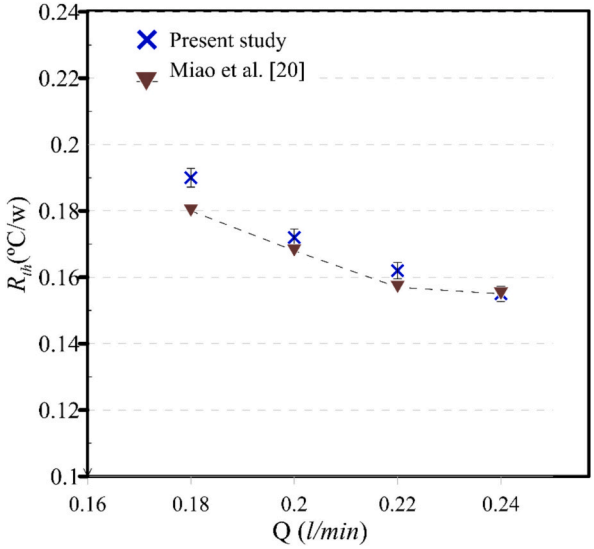

Fig. 3. Validation of plain cooled plate.

3. Data processing

The impact of microchannel geometry and the implementation of the jet impingement cooling method is evaluated by examining thermal and hydraulic parameters, including thermal resistance, Nusselt number, surface temperature, as well as fanning friction factor. The heat transfer rate (Q) within the microchannel is determined using the working fluid flow rate and the inlet and outlet fluid temperatures, and is calculated as follows [18,19]:

$$Q = \dot{m}C_p(T_i - T_o) \tag{1}$$

Once the Q is determined, the thermal resistance can be calculated using Eq. (2) [20,21].

$$R_{th} = \frac{\Delta T}{Q} \tag{2}$$

Where:

$$\Delta T = \left(T_{s,avg} - T_{w,avg}\right) - (T_i - T_o) \tag{3}$$

In this equation, $T_{s,avg}$ represents the average surface temperature, and $T_{w,avg}$ denotes the mean fluid temperature, both of which are obtained from Eqs. (4) and (5), respectively [18,19,21].

$$T_{w,avg} = \frac{T_i + T_o}{2} \tag{4}$$

$$T_{s,avg} = \frac{T_{s,1} + T_{s,2} + T_{s,3} + T_{s,4}}{4} \tag{5}$$

Using Eqs. (2) to (5), the thermal resistance equation can be rewritten as follows [20]:

$$R_{th} = \frac{T_{s,avg} - T_i + 0.5(T_o - T_i)}{Q} \tag{6}$$

The convective heat transfer coefficient of the microchannel (h) is also calculated using Eq. (7) [18,19,21].

$$h = \frac{Q}{LW(T_{s,avg} - T_{w,avg})} \tag{7}$$

In this equation, the microchannel's dimensions are denoted by L and W, corresponding to a length of 4 cm and a width of 6 cm in the current study. Moreover, the Nusselt and Reynolds numbers are calculated based on the following expressions [18,19]:

$$Nu = \frac{hD_h}{k} \tag{8}$$

$$Re = \frac{\rho u D_h}{\mu} \tag{9}$$

Where [18],

$$D_h = \frac{4A_c}{l} \tag{10}$$

In these equations, l denotes the microchannel's wetted perimeter.

Heat transfer enhancement techniques, such as incorporating microchannels on the cold plate surface and employing jet impingement cooling, affect not only thermal parameters but also pressure drop. Therefore, in addition to evaluating heat transfer and thermal resistance, the fanning friction factor, calculated using Eq. (11), has been assessed as a dimensionless indicator of pressure loss. To determine the optimal configuration, the thermal enhancement factor (TEF), obtained from Eq. (12), was employed as a dimensionless metric that simultaneously accounts for variations in both heat transfer and pressure drop [19,20,22,23].

$$f = \frac{D_h(P_i - P_o)}{2\rho L u^2} \tag{11}$$

$$TEF = \frac{\frac{Nu}{Nu_p}}{\left(\frac{f}{f_p}\right)^{1/3}} \tag{12}$$

Where f_p and Nu_p indicate the plain cold plate friction factor and Nusselt number, respectively.

4. Results and discussion

4.1. Validation and uncertainty analyses

To ensure the reliability of the experimental methodology, the thermal resistance of the plain cold plate investigated in this study was benchmarked against previously published data by Miao et al. [20]. The comparison demonstrates a high degree of consistency, with maximum deviations not exceeding 5.8%. This validation provides confidence that subsequent results obtained for different microchannel geometries and cooling strategies accurately reflect the thermal performance under the tested conditions.

To ensure the reliability of the experimental findings, a comprehensive uncertainty analysis was performed. Inherent limitations of measurement instruments and random variations in the experimental process introduce unavoidable uncertainties in laboratory studies. The results uncertainty was decomposed into two main categories. Type A uncertainty, reflecting the statistical variation in repeated measurements, was quantified according to the standard deviation formula outlined in Eq. (13) [20]. Type B uncertainty, capturing systematic deviations associated with the calibration and accuracy of the instruments, was estimated following Eq. (14) [20]. The combined influence of both uncertainty sources was then integrated to obtain the overall measurement uncertainty, as described by Eq. (15) [20]. The quantified uncertainties for all measured parameters are summarized in Table 1, providing a clear assessment of the confidence level in the reported experimental data.

$$u_A = \sqrt{\frac{\sum_{i=1}^{n}(N_i - \overline{N})^2}{n(n-1)}} \tag{13}$$

$$u_B = \frac{\Delta m}{\sqrt{C}} \tag{14}$$

$$U = \sqrt{\sum_{i=1}^{n} u_{A,i}{}^2 + \sum_{j=1}^{n} u_{B,j}{}^2} \tag{15}$$

In the above equations, N_i represents the individual measured value, N denotes the arithmetic mean of all measurements, n is the number of repeated trials, and Δm corresponds to the accuracy specification of the instrument. The factor C refers to the distribution coefficient associated with the measurement error of the device, which is commonly taken as 3.20.

Table 1
Measurement uncertainty and instrument accuracy.

Uncertainty and accuracy of the measurement instruments		
Measurement instruments	Accuracy	Uncertainty
Turbine-type flow meter	±0.1%	0.0577
Data logger	±0.5%	0.288
k-type thermocouple	±0.5%	0.288
Pressure gauge	±2%	1.7

The overall measurement uncertainty	
Parameter	Uncertainty
Nusselt number	5.6%
Friction factor	7.8%
Reynolds numbers	3.5%
Thermal resistance	4.3%

4.2. Effect of microchannel geometry

The first part of this study aims to evaluate the influence of microchannel geometry on the thermal and hydraulic performance of the cold plate. To this end, three geometries—rectangular, arc-shaped, and sinusoidal—were designed and compared with a simple cold plate under different TDP levels of 500, 750, and 1000 W. The working fluid was introduced into the microchannel using the single-inlet method, and all experiments were conducted at a constant inlet temperature of 25 °C with flow rates ranging from 1 to 4 *l*/min, enabling a simultaneous assessment of geometric and operating-condition effects. The results of this evaluation are presented in Figs. 4–6.

The findings indicate that incorporating microchannels into the cold plate significantly reduces thermal resistance and enhances heat-transfer performance compared with the simple cold plate. As shown in Fig. 4a and b, at a flow rate of 1 *l*/min and a TDP of 500 W, the thermal resistance of the rectangular, arc-shaped, and sinusoidal microchannels is reduced by 4.1%, 5.0%, and 6.3%, respectively, relative to the simple cold plate, while the Nusselt number increases by 4.8%, 5.9%, and 7.5%. Moreover, the influence of geometry becomes more pronounced at higher flow rates and TDP levels. For example, at a TDP of 1000 W and a flow rate of 4 *l/min*, the thermal resistance of the rectangular, arc-shaped, and sinusoidal microchannels decreases by 8.2%, 9.4%, and 10.9%, respectively, compared with the simple cold plate, while the Nusselt number increases by 11.3%, 13.2%, and 15.7%. The enhancement in thermal performance resulting from the incorporation of microchannels on the cold plate arises from a combination of physical mechanisms that simultaneously influence heat transfer and flow behavior. First, the introduction of microchannels significantly increases the effective heat-transfer surface area, as multiple walls are exposed to the flow, thereby substantially enlarging the convective surface. This increase in surface area is a primary reason for the superior thermal performance of microchannels compared with the simple cold plate. Second, while flow in a simple cold plate predominantly follows a straight path from inlet to outlet, the microchannel structure induces continuous interactions between the fluid and surface protrusions and bends. These interactions generate secondary flows and enhance fluid mixing, which suppresses the growth of the thermal boundary layer and improves convective heat transfer. Another contributing factor is the reduction of conductive path length due to microchannel machining. In a simple cold plate, the greater thickness leads to higher conductive resistance, whereas the presence of microchannels shortens the conduction path, allowing heat to be transferred more rapidly to the fluid. Among the investigated geometries, the sinusoidal microchannel exhibits the best performance. Its curved pathway induces secondary flows and enhances local fluid mixing. Additionally, the continuous change in flow direction generates periodic detachments from the walls—phenomena absent in the simple and rectangular cold plates, where the flow remains predominantly unidirectional and weakly mixed. The effect of flow rate is similarly associated with increased fluid velocity. At a given geometry (fixed hydraulic diameter), higher flow rates elevate the velocity, reducing the thermal boundary-layer thickness and consequently decreasing thermal resistance while increasing the Nusselt number.

In high-performance processors with elevated TDPs, controlling the surface temperature is a critical design requirement. The surface temperature not only serves as a direct indicator of cooling effectiveness but also plays a fundamental role in reliability, operational stability, and chip longevity. Processors typically have a defined allowable temperature range, the Thermal Design Limit, which the surface temperature

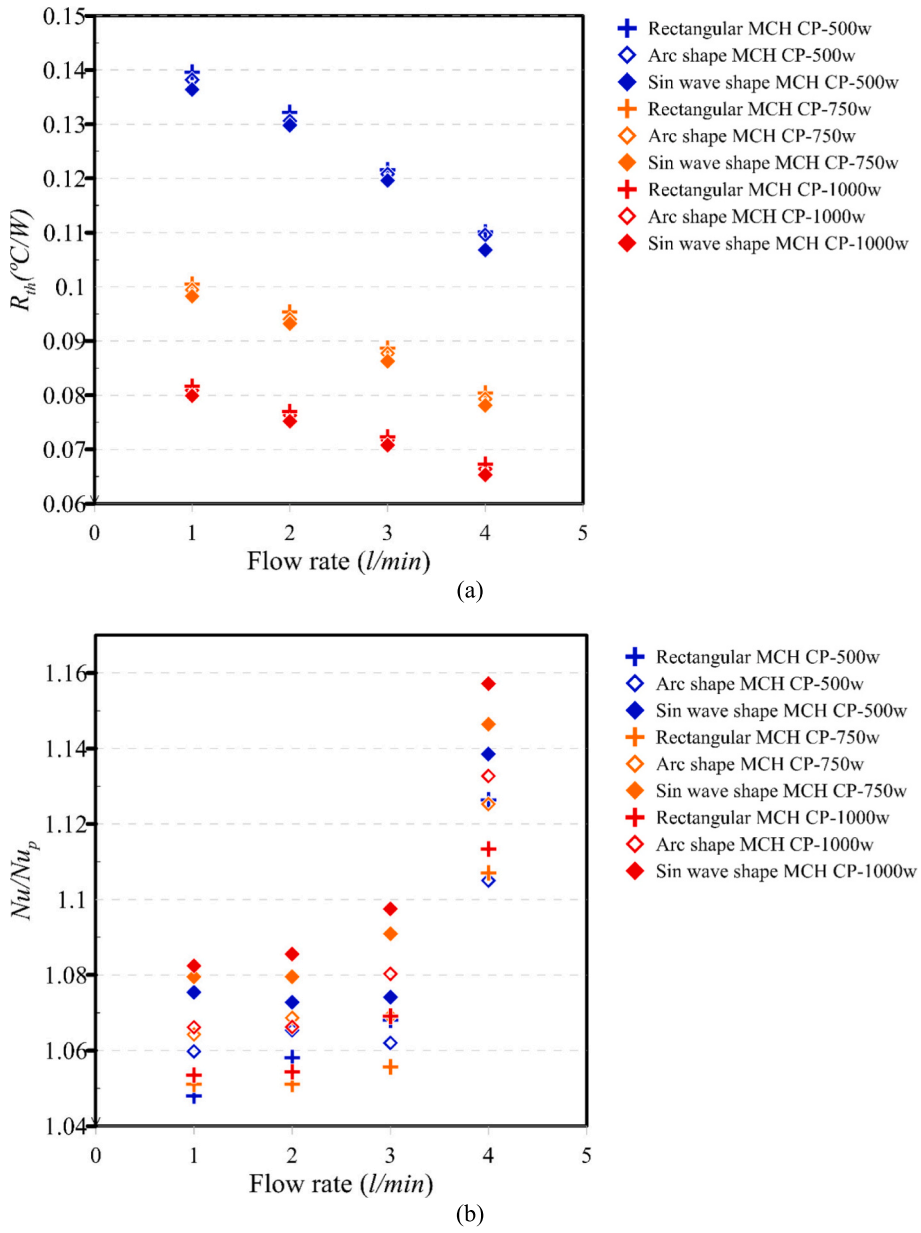

Fig. 4. Effect of microchannel geometry on the thermal resistance (a), Nu/Nu_p (b), and surface temperature(c).

should not exceed. For many modern CPUs, this limit ranges between 80 and 95 °C; in this study, a threshold of 85 °C is adopted to evaluate cooling performance. Fig. 4c shows the variation of surface temperature with fluid flow rate for the simple cold plate and microchannels with rectangular, arc-shaped, and sinusoidal geometries under TDPs from 500 to 1000 W. The results indicate that for the simple cold plate at TDPs of 500, 750, and 1000 W, the surface temperature at 1 *l*/min is 94.2, 98.3, and 103.1 °C, respectively, while at 4 *l/min* it is 81.2, 85.2, and 91.1 °C. These values demonstrate that the simple cold plate can only meet cooling requirements at low TDPs and relatively high flow rates (4 *l/min*), whereas at high heat loads and across all flow rates, the surface temperature exceeds the critical threshold of 85 °C. In contrast, replacing the simple cold plate with rectangular, arc-shaped, or sinusoidal microchannels significantly reduces the surface temperature. At a TDP of 1000 W, depending on the flow rate, the surface temperature for rectangular, arc-shaped, and sinusoidal geometries ranges from 85 to 99.5 °C, 84.2 to 98.7 °C, and 83.1 to 97.7 °C, respectively. The lowest surface temperature is observed for the sinusoidal geometry, which can reduce the surface temperature by up to 5.4 °C at 1 *l*/min and 8 °C at 4 *l/min* compared with the simple cold plate. Despite these advantages, the results indicate that although the sinusoidal microchannel cold plate can deliver adequate performance at high TDPs with 4 *l*/min flow, it is insufficient to maintain surface temperatures below 85 °C at low flow rates.

In addition to enhancing thermal performance, the incorporation of microchannels also affects pressure loss and the friction factor. Fig. 5 illustrates the variation of friction factor with fluid flow rate for the simple cold plate and different microchannel geometries. The results indicate that at a flow rate of 1 *l*/min, the rectangular, arc-shaped, and sinusoidal microchannels increase the friction factor by 1.10, 1.12, and 1.14 times, respectively, compared with the simple cold plate. Moreover, the influence of microchannel incorporation on the friction factor diminishes as the flow rate increases. For instance, at a flow rate of 4 *l/min*, the friction factor for the same microchannels is observed to be 1.04, 1.06, and 1.08 times that of the simple cold plate. The increase in friction factor observed in microchannel cold plates compared with the

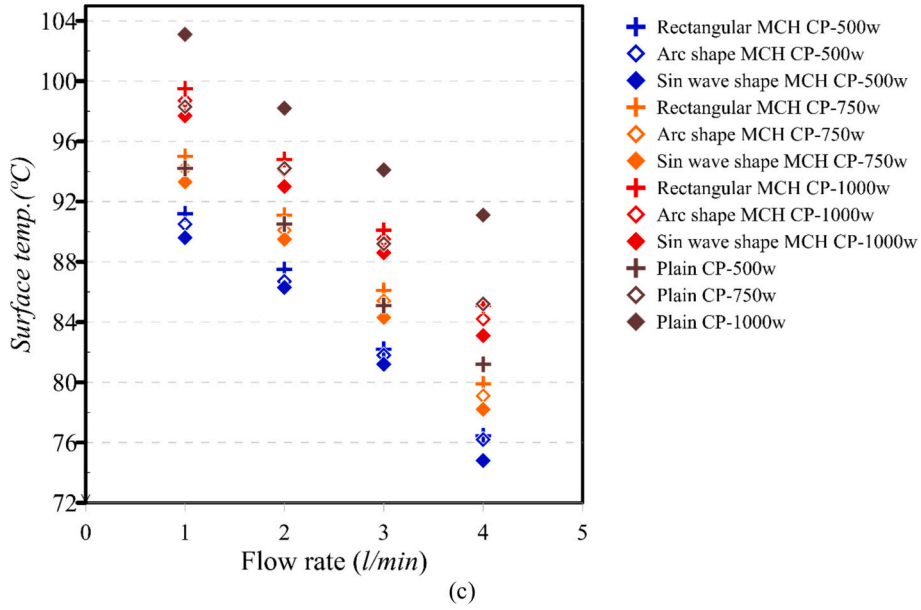

Fig. 4. (*continued*).

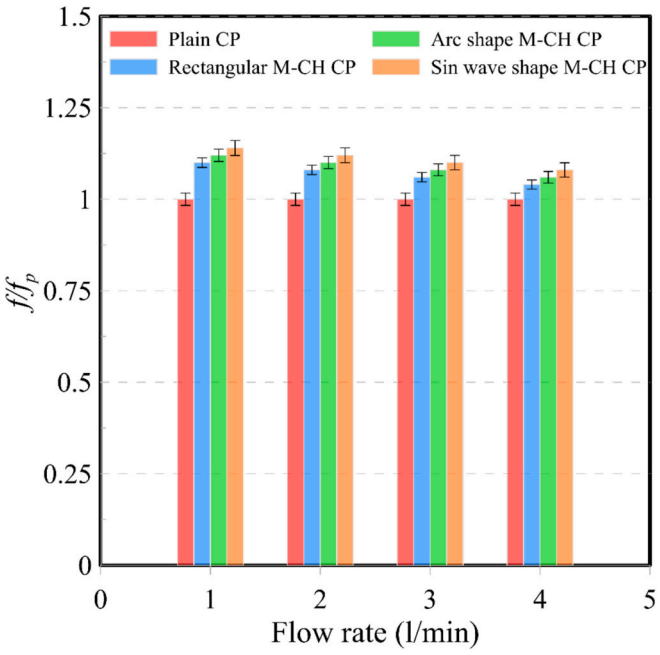

Fig. 5. Effect of microchannel geometry on the f/f_p.

simple cold plate is primarily due to the enlarged wetted surface area. The introduction of microchannels increases the contact area between the fluid and the cold plate walls, naturally leading to higher friction-induced pressure loss. Additionally, the geometric structure of the microchannels—particularly the sinusoidal geometry—generates multi-directional flows and secondary vortices. This local disturbance and the resulting increase in turbulence further elevate the friction factor relative to the simple cold plate.

The incorporation of microchannels on the cold plate simultaneously enhances heat transfer and increases pressure loss. Therefore, the selection of an optimal geometry must balance these opposing effects: improved heat transfer is desirable, whereas an increased friction factor is unfavorable. To assess these two parameters concurrently, the thermal–hydraulic efficiency factor (TEF) is employed, with its variation against flow rate for all geometries presented in Fig. 5. The results indicate that at a TDP of 500 W and a flow rate of 1 *l*/min, the TEF values for the rectangular, arc-shaped, and sinusoidal microchannels are 1.015, 1.02, and 1.03, respectively. This demonstrates that the sinusoidal geometry not only provides superior thermal performance but also exhibits the best thermo-hydraulic efficiency based on the TEF metric. Furthermore, the results show that TEF increases with higher TDP and flow rate. For example, at a TDP of 1000 W and a flow rate of 4 *l/min*, the TEF of the sinusoidal microchannel reaches 1.13, indicating a significant improvement in its hydrothermal performance under high heat load and high flow conditions.

4.3. *Effect of jet impingement cooling*

Based on the results presented in the previous section, the simple cold plate was unable to meet cooling requirements at high TDPs (e.g., 1000 W) across all examined flow rates, with surface temperatures exceeding 85 °C in every case. The sinusoidal microchannel, which exhibited the best thermal and hydrothermal performance among the studied geometries, could only maintain surface temperatures below 85 °C at a flow rate of 4 *l*/min. In the second phase of the study, to further enhance thermal performance, the fluid delivery method was modified: instead of the single-inlet method, cooling was implemented using jet impingement. The effect of this method on thermal parameters for the simple cold plate as well as the various microchannel geometries is presented in Fig. 7.

According to Figs. 7(a) and 7(b), the application of jet impingement on the simple cold plate reduces thermal resistance while increasing the Nusselt number. At a flow rate of 1 *l*/min and a TDP of 500 W, jet impingement lowers the thermal resistance of the simple cold plate by 1.4% and increases the Nusselt number by 1.6%. As the flow rate and TDP increase, the effect of jet impingement intensifies, such that at 4 *l/min* and a TDP of 1000 W, this cooling method reduces thermal resistance by 12.8% and enhances the Nusselt number by 19%. Furthermore, combining jet impingement with rectangular, arc-shaped, and sinusoidal microchannels under the same operating conditions results in reductions of thermal resistance by 10.1%, 11.2%, and 12.3%, respectively, and increases in the Nusselt number by 14.7%, 16.6%, and 18.7% compared with the single-inlet method. In other words, the highest thermal performance observed in this study is achieved by employing jet impingement in conjunction with the sinusoidal

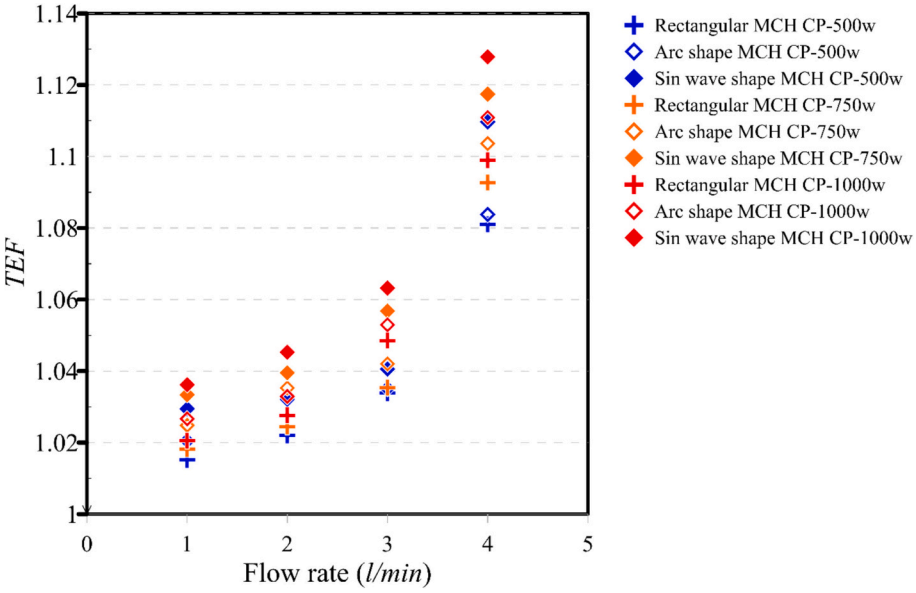

Fig. 6. Effect of microchannel geometry on the TEF.

microchannel, which exhibits a thermal resistance up to 21.8% lower and a Nusselt number up to 37.3% higher than the simple cold plate.

The enhancement of heat transfer and reduction of thermal resistance in jet impingement cooling are strongly determined by the flow structures within the microchannels. When high-velocity fluid exits the nozzle and strikes the surface, a high-pressure, focused flow region is formed. This impact disrupts the thermal boundary layer, causing a significant local reduction in thermal resistance. At the impingement point, the combination of high fluid velocity and low temperature maximizes the wall-to-fluid temperature difference, thereby enhancing convective heat transfer and substantially increasing the local Nusselt number. After impingement, the fluid spreads along the surface as a strong wall jet. With high momentum, this wall jet modifies the near-wall flow, weakening both the velocity and thermal boundary layers. This phenomenon leads to increased mixing in the flow, which in turn intensifies turbulence and further enhances the heat-transfer rate in the regions surrounding the impingement zone. The effectiveness of jet impingement is further amplified at higher flow rates due to the increased velocity of the ejected fluid. As the discharge from each nozzle rises while the nozzle cross-section remains constant, the impingement velocity on the cold plate increases. This intensifies the influence of the jet on local flow patterns and wall jets, ultimately improving overall thermal performance.

The reduction in thermal resistance and the increase in the Nusselt number resulting from jet impingement cooling lead to a significant decrease in surface temperature. The effect of this method on surface temperature becomes more pronounced with higher TDP and flow rates. For instance, at a flow rate of 4 *l*/min and a TDP of 1000 W, jet impingement lowers the surface temperature of the simple cold plate, and the rectangular, arc-shaped, and sinusoidal microchannels to 81.7, 78.3, 76.8, and 75.1 °C, respectively. These values correspond to reductions of 9.4, 6.9, 7.4, and 8 °C compared with the single-inlet method. Another key advantage of combining microchannels with jet impingement is the reduction in the minimum flow rate required to achieve a safe surface temperature. For example, at a TDP of 1000 W, the simple cold plate maintains surface temperatures above 85 °C across all examined flow rates. With jet impingement, however, the surface temperature reaches 81.7 °C at 4 *l/min*, falling within the acceptable range. The sinusoidal microchannel, which provided the best thermal performance under the single-inlet method, achieved surface temperatures below 85 °C only at 4 *l/min*. By employing jet impingement, the sinusoidal microchannel reaches 80.3 °C at 3 *l/min*, remaining below the 85 °C threshold. In summary, jet impingement enables achieving desirable surface temperatures at lower flow rates, with further details provided in Table 2.

The results from the experiments also demonstrated that the jet impingement effect in the cold plate microchannel with a sinusoidal design is more pronounced than in the cold plate with a simple design and other microchannel configurations. The superiority of the sinusoidal geometry is attributed to its distinctive curvature and changes in cross-section, which cause the nozzle outlet flow to deviate in various directions. These deviations, along with the wall jets that are formed, contribute to the generation of secondary flows. This complex and multidirectional flow structure increases turbulence and promotes effective mixing, while the combined effect of the sinusoidal geometry and the jet impingement mechanism leads to a notable enhancement in heat transfer relative to other geometries; a phenomenon that is less frequently observed in simpler geometries.

Fig. 8 presents the variation of friction factor with coolant flow rate for all cases under jet impingement. The results show that, in addition to improving thermal performance, this cooling method increases both the friction factor and the pressure loss. The rise in pressure loss primarily originates from the flow acceleration through the narrow jet nozzle and the abrupt changes in velocity and pressure. As the coolant is forced through the small nozzle opening, its velocity increases significantly, which—according to the Bernoulli relation—reduces the static pressure and intensifies the overall pressure loss. After exiting the nozzle, the jet expands into a larger cross-sectional area, leading to flow separation and the formation of local vortices, both of which increase local losses and consequently the total pressure loss. Furthermore, the high-momentum jet impact induces strong mixing and hydrodynamic instabilities near the impingement region, contributing further to energy dissipation and pressure loss. For these reasons, the pressure loss in the jet impingement configuration is substantially higher than that of the single-inlet method. Based on the results, applying jet impingement increases the friction factor of the plain cold plate and the rectangular, arc-shaped, and sinusoidal microchannels at 1 *l*/min to 1.18, 1.145, 1.15, and 1.148 times, respectively, compared to the single-inlet method. At 4 *l/min*, the friction factor increases to 1.12, 1.165, 1.16, and 1.15 times for the same cases.

In addition to increased pressure loss, jet impingement enhances the TEF. The maximum TEF reported in this study is 1.278, occurring at

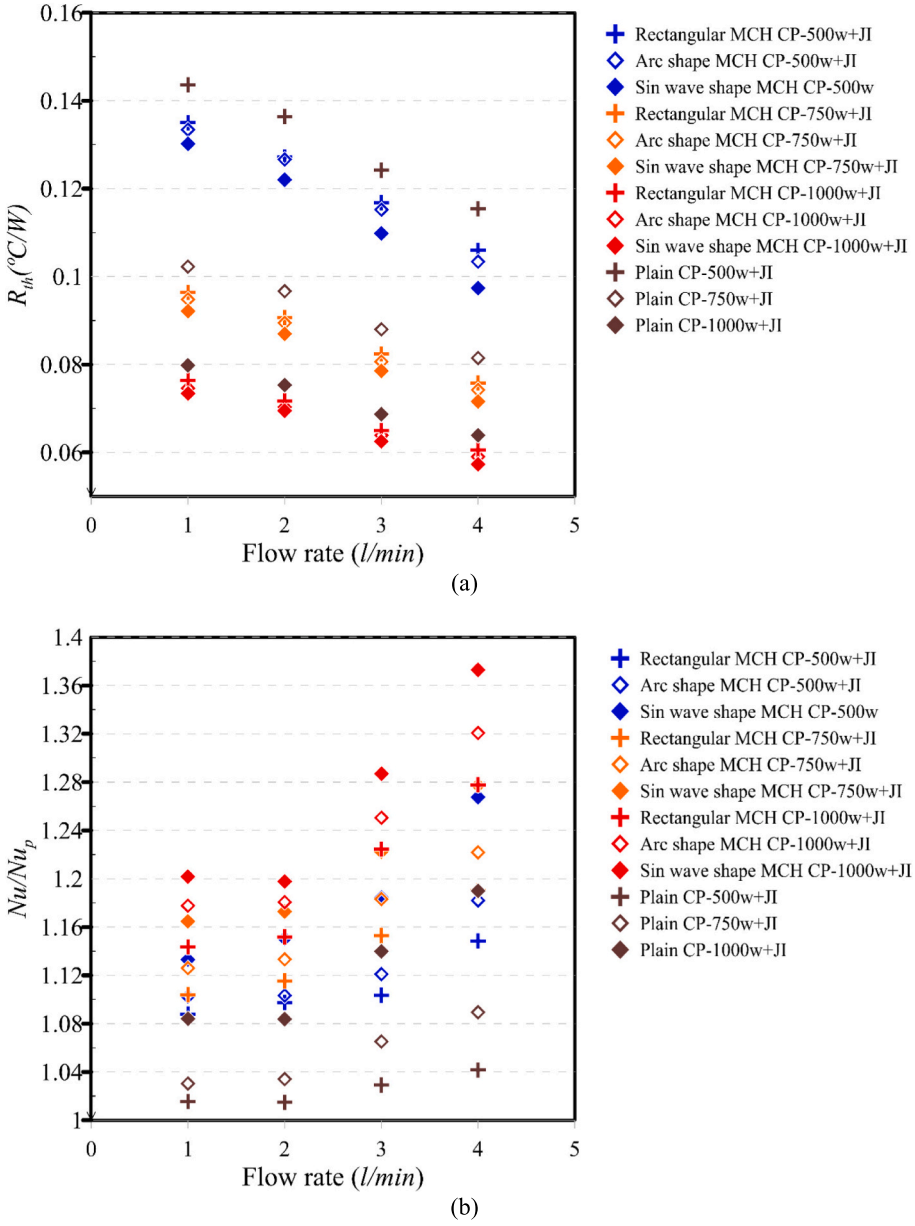

Fig. 7. Effect of hybrid microchannel and internal jet impingement cooling on the thermal resistance (a), Nu/Nu_p (b), and surface temperature(c).

TDP = 1000 W and 4 *l/min* for the sinusoidal microchannel under jet impingement. This value is 13.3% higher than that of the sinusoidal microchannel operating with the single-inlet method, indicating that the combination of sinusoidal geometry and jet impingement yields the highest hydrothermal performance.

In addition, a comparative assessment has been performed between the present study and previously reported works (Table 2). For this purpose, the results of the current study are categorized into four configurations: a plain cold plate with a single-inlet configuration, a sinusoidal microchannel with a single-inlet configuration, a plain cold plate with internal jet impingement, and the combined configuration of a sinusoidal microchannel with internal jet impingement. The comparison is conducted in terms of thermal resistance as a common performance metric, enabling a clear and consistent evaluation of the relative performance of the proposed approach against existing cooling strategies.

4.4. Energy reuse capability

In modern data centers, the deployment of numerous CPUs and GPUs leads to substantial coolant flow rates in liquid cooling systems, particularly within microchannels. The high heat transfer efficiency of these channels results in elevated fluid temperatures and energy at the outlet. Recovering this thermal energy before discharging it to the secondary reservoir can significantly improve overall system efficiency. To evaluate the feasibility of heat recovery and the effects of microchannel geometry and fluid delivery methods, the outlet flow from the microchannels is assumed to feed a heat pump operating on an ideal Carnot cycle, raising the fluid temperature to 70 °C. In this framework, the microchannel outlet temperature is treated as the evaporator temperature, while the condenser temperature is fixed at 70 °C. The cycle's coefficient of performance (COP) is calculated using Eq. (16) [25], with its dependence on the heat pump inlet temperature (i.e., the microchannel outlet temperature) illustrated in Fig. 9. Here, T_c and T_{ev} represent the condenser (heat pump outlet) and evaporator (microchannel outlet)

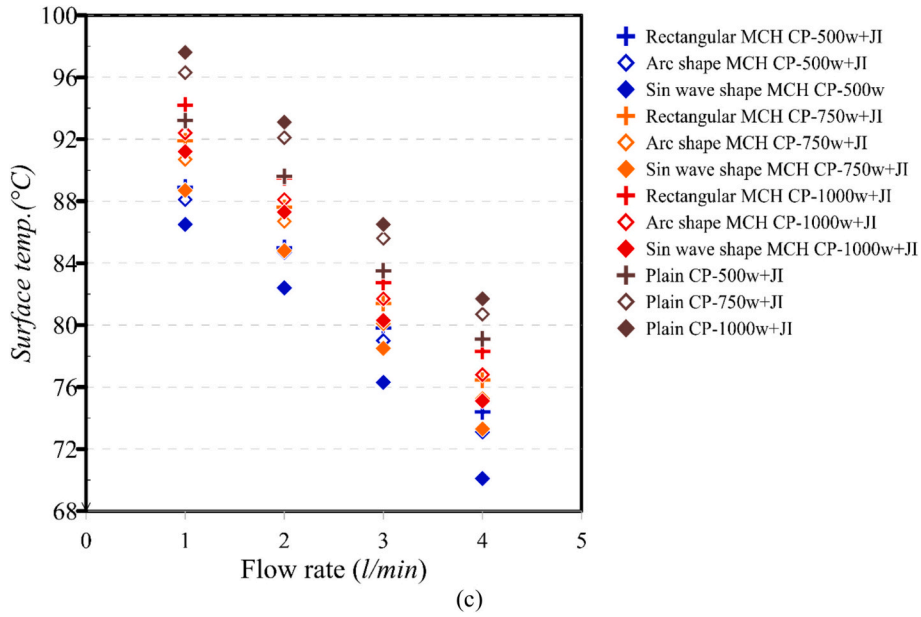

Fig. 7. (*continued*).

Table2
A comparative illustration of the current study alongside similar studies regarding the R_{th}.

Researcher	Detail	Flow rate (l/min)	R_{th} (°C/W)
M. Shanmugam et al. [21]	Microchannel with different flow configurations	0.25	0.174–0.42
Jie Miao et al. [20]	Microchannels featuring side wall ribs and bottom cavities	0.16–0.24	0.15–0.24
Elliott and Robinson [13]	Traditional jet impingement	1–7	1.52–1.78
R. Xiao et al. [24]	Microchannel with traditional jet impingement	0.86–1.9	0.11–0.24
Present study	Plain cold plate with single-inlet configuration	1–4	0.073–0.145
Present study	Sinusoidal microchannels with single-inlet configuration	1–4	0.065–0.136
Present study	Plain cold plate with internal JI	1–4	0.064–0.143
Present study	Sinusoidal microchannels with internal JI	1–4	0.057–0.13

temperatures, respectively. The results reveal a strong correlation between COP and inlet temperature: as the inlet temperature increases, COP rises. It should be noted that the COP considered in this study does not represent the actual performance of a real heat pump system, as it does not include mechanical work inputs such as pumping power. Instead, the Carnot-based COP is employed as an idealized thermodynamic upper bound to evaluate the relative energy recovery potential of the coolant. This formulation enables a consistent comparison between different cooling configurations based on the outlet temperature level, which governs the quality of the recoverable thermal energy. Also, the Energy Reuse Factor (ERF) is determined using Eq. (17), where η_{reuse} is taken as the heat pump COP, assuming identical captured energy ($Q_{captured}$) and total data center energy consumption across all scenarios. Under this assumption, COP directly corresponds to ERF.

$$COP = T_c/(T_c - T_{ev}) \tag{16}$$

$$ERF = \left(Q_{captured}{}^{*}\ \eta_{reuse}\right)/(\text{Total Data Center Energy consumption}) \tag{17}$$

For a detailed assessment, experiments were conducted on a simple cold plate and microchannels of various geometries, using both single-inlet and jet impingement methods. At a TDP of 1000 W, the coolant flow rate was initially set to 1 *l/min*, and the surface temperature was recorded. The flow rate was then increased gradually until the surface temperature reached the safe limit of 85 °C. This condition defines the minimum flow rate needed to maintain safe surface temperatures while achieving the maximum microchannel outlet temperature, as reported in Table 2. Using Eqs. (16) and (17) together with the data in Table 3, ERF values for the different configurations were calculated, and the improvement relative to the simple cold plate is presented in Fig. 11.

According to the results, the minimum flow rates required to maintain a safe surface temperature for the simple cold plate, rectangular, arc-shaped, and sinusoidal microchannels using the single-inlet method are 6.3, 3.95, 3.6, and 3.32 *l*/min, respectively. At these flow rates, the corresponding outlet temperatures of the working fluid are 27.3, 28.6, 29.1, and 29.45 °C, respectively. When employing jet impingement cooling, the minimum flow rates are reduced to 3.1, 2.8, 2.55, and 2.2 *l/min*, with outlet temperatures rising to 29.6, 30.2, 30.8, and 31.5 °C, respectively. These results demonstrate that heat transfer enhancement techniques reduce the minimum flow rate required to maintain a safe surface temperature. Consequently, for a given heat load and fixed inlet temperature, the microchannel outlet temperature increases, which—according to Eqs. (16) and (17) and as shown in Fig. 10—leads to higher COP and, consequently, higher ERF. As illustrated in Fig. 11, the sinusoidal microchannel, representing the optimal geometry, achieves an ERF increase of up to 5.2% relative to the simple cold plate when using the single-inlet method. Combining the sinusoidal geometry with jet impingement further enhances ERF, achieving an increase of up to 11%. These findings indicate that employing heat transfer enhancement strategies can effectively improve the energy reuse efficiency in such systems.

5. Conclusion

In this study, a hybrid cooling architecture was introduced for the first time, combining geometrically optimized microchannels with an internal jet impingement system. The effects of various parameters, including cold plate geometry, working fluid flow rate, TDP, and the fluid entry configuration into the microchannels, were comprehensively evaluated on both thermal and hydraulic performance. The key findings

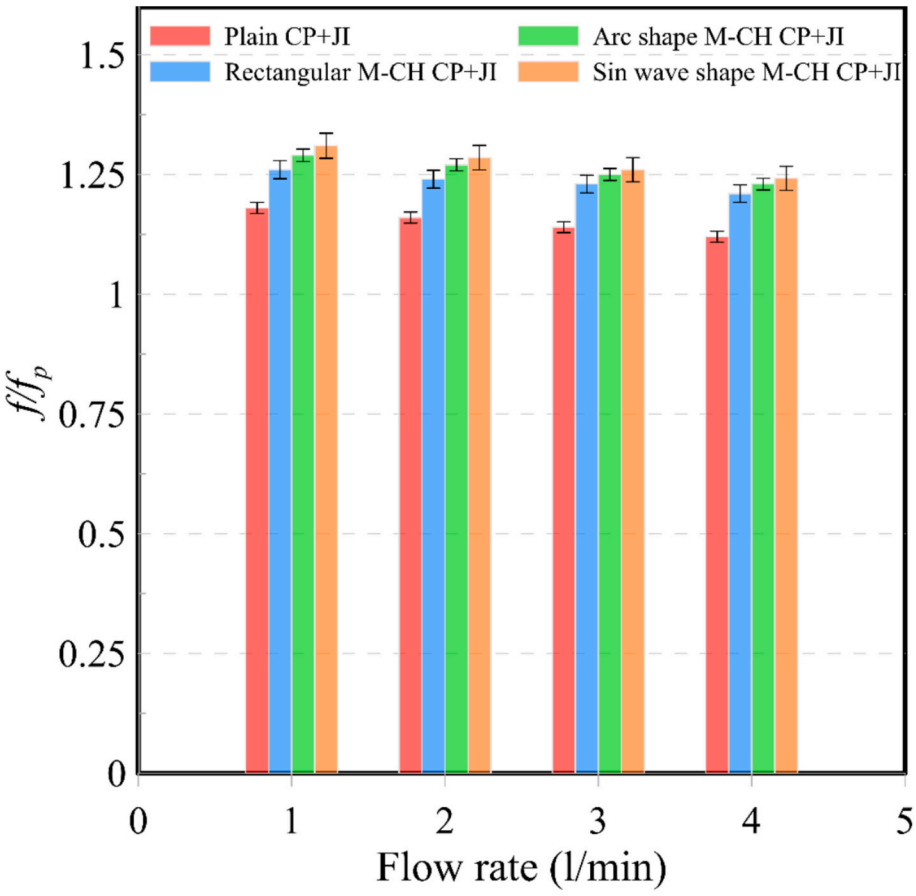

Fig. 8. Effect of hybrid microchannel and internal jet impingement cooling on the f/f_p.

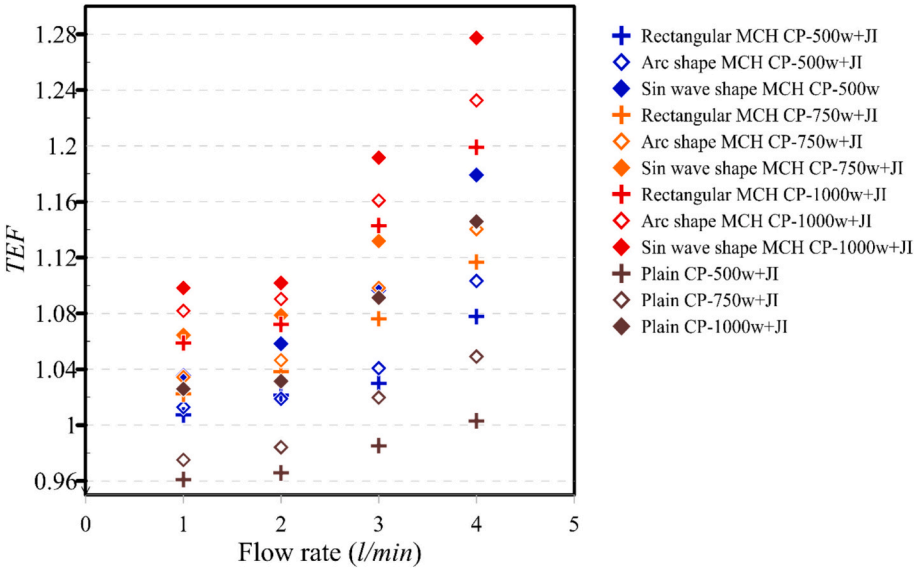

Fig. 9. Effect of hybrid microchannel and internal jet impingement cooling on the TEF.

are summarized as follows:

- Implementation of microchannels significantly reduced thermal resistance compared to a plain cold plate. For instance, at a flow rate of 1 *l*/min and TDP = 500 W, thermal resistance decreased by 4.1%, 5.0%, and 6.3% for rectangular, semicircular, and sinusoidal geometries, respectively; these reductions increased to 8.2%, 9.4%, and 10.9% at 4 *l*/min and TDP = 1000 W.
- The sinusoidal geometry exhibited the best overall performance across all metrics. Under the highest test conditions (TDP = 1000 W, 4 *l/min*), the Nusselt number increased by 15.7% and the surface temperature decreased by 8 °C compared to a plain cold plate.

Table 3
Flow rate versus cooling block outlet temperature.

Selected Scenario	TJ safe Temp.(°C)	Corresponding flow rate (l/min)	Corresponding Outlet temp. (°C)
Plain CP	85	6.3	27.3
Rectangular M-Ch CP	85	3.95	28.6
Arc Shape M-Ch CP	85	3.6	29.1
Sin wave shape M-Ch CP	85	3.32	29.45
Plain CP + JI	85	3.1	29.6
Rectangular M-Ch CP + JI	85	2.8	30.2
Arc Shape M-Ch CP + JI	85	2.55	30.8
Sin wave shape M-Ch CP + JI	85	2.2	31.5

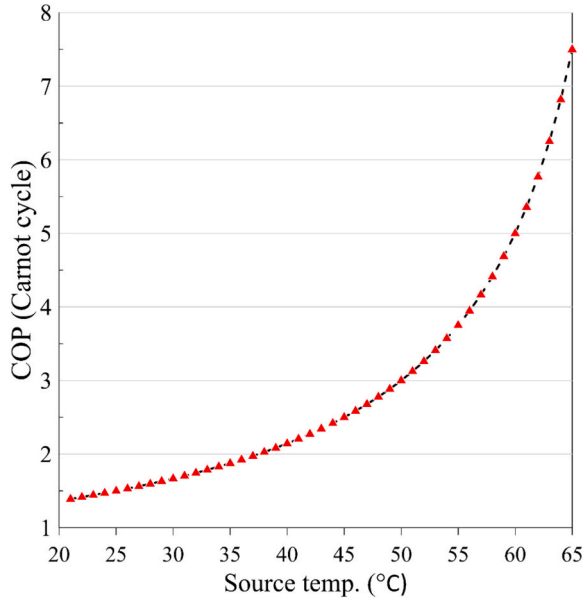

Fig. 10. Variation of COP for a Carnot heat pump with respect to source temperature.

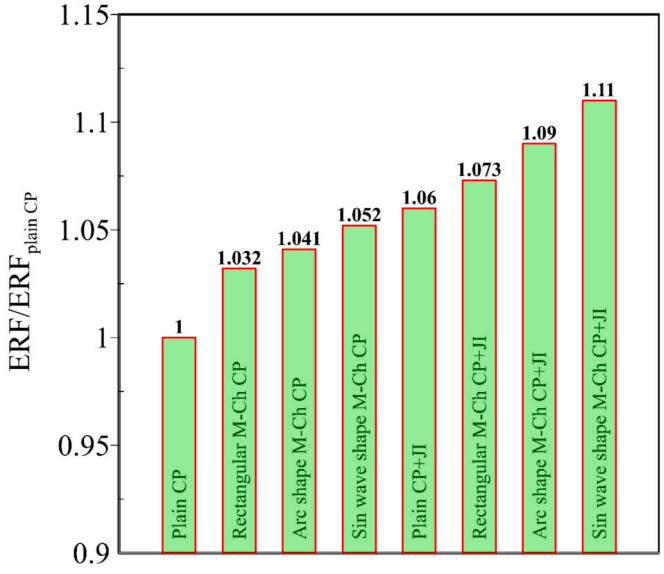

Fig. 11. Variation of $ERF/ERF_{plain\ CP}$ among the analyzed configurations.

- Adding jet impingement to a plain cold plate reduced thermal resistance by up to 12.8% and increased the Nusselt number by 19%. This effect was further enhanced when combined with microchannels, achieving a 21.8% reduction in thermal resistance and a 37.3% increase in Nusselt number for the sinusoidal geometry—the highest values recorded in the study.
- The hybrid configuration of jet impingement with microchannels also substantially lowered surface temperatures. At TDP = 1000 W and 4 *l*/min, the sinusoidal microchannel temperature reached 75.1 °C, representing a 16 °C decrease compared to the plain cold plate.
- Although jet impingement increased pressure drop, it simultaneously improved the TEF index. The maximum TEF of 1.278 was observed in the sinusoidal geometry at TDP = 1000 W and 4 *l/min*, representing a 13.3% improvement over the single-inlet configuration.
- Heat transfer enhancement methods reduced the minimum flow rate required to maintain the surface temperature within the safe range (85 °C). At TDP = 1000 W, the minimum flow rates for plain, rectangular, semicircular, and sinusoidal cold plates in the single-inlet mode were 6.3, 3.95, 3.6, and 3.32 *l/min*, respectively, which decreased to 3.1, 2.8, 2.55, and 2.2 *l/min* when jet impingement was applied. This reduction in flow rate increased outlet fluid temperature and further enhanced energy recovery capacity.
- The highest ERF was observed in the sinusoidal geometry, showing a 5.2% improvement over the plain cold plate in single-inlet mode and up to 11% improvement in the hybrid configuration with jet impingement.

Overall, this hybrid architecture presents a promising approach for designing high-performance, energy-efficient cooling systems.

5.1. Limitations and suggestions for future studies

The present study was conducted on a cold plate with an effective area of 40 × 60 mm, which is representative of typical high-performance CPU and GPU packages. The proposed hybrid architecture—combining geometrically optimized microchannels with an internal jet impingement manifold—exhibits inherent scalability. For larger chip dimensions, the design can be extended by replicating the fundamental unit consisting of a branch manifold with four jet nozzles and the corresponding microchannel segment. The modular nature of the jet delivery system allows straightforward scaling by increasing the number of branches while maintaining a consistent nozzle-to-surface distance and jet density. This approach preserves the local thermal-hydraulic enhancement mechanisms observed in this study. For applications with higher heat fluxes (e.g., > 1000 W), new studies can be conducted to evaluate the cooling capacity by increasing the flow rate per nozzle or by reducing nozzle diameter to elevate jet velocity, albeit with a corresponding increase in pumping power. Alternatively, the nozzle density can be increased by reducing the spacing between branches, provided that the associated pressure drop remains within system constraints. The current results, obtained over a flow rate range of 1–4 *l*/min and heat loads up to 1000 W, demonstrate a wide operational envelope; extrapolation to larger or more power-dense devices is therefore feasible through conservative design rules based on maintaining constant jet Reynolds number or constant pumping power per unit area. Further scaling studies involving full-sized prototypes and system-level thermal-fluid simulations would be valuable to validate these projections.

CRediT authorship contribution statement

Sultan Alshehery: Writing – original draft, Software, Funding acquisition, Conceptualization. **Dan Dobrotă:** Writing – original draft, Validation. **Augustin Stoica:** Writing – original draft, Software, Resources. **Hussain Sawwan:** Writing – review & editing, Formal analysis. **Salman Saeidlou:** Writing – review & editing, Formal analysis, Data

curation. **Nemat Mashoofi Maleki:** Writing – original draft, Investigation. **Ibrahim Mahariq:** Writing – review & editing, Supervision.

Declaration of competing interest

The authors clarified that they have no conflicts of interest.

Acknowledgment

This research was funded by the Deanship of Research and Graduate Studies at King Khalid University under grant number RGP.2/737/46.

Appendix A. Appendix

In this section, a detailed examination of one of the flow rates (flow rate = 1 *l/min*) is conducted concerning surface temperatures. The T_{s1}-T_{s4}, in relation to the cold plate, are presented in Table 4. It is evident that temperatures T_{s1} and T_{s2} are quite similar, indicating that the temperatures in the cross sections are nearly identical due to symmetry, whereas T_{s3} and T_{s4} are considerably higher than T_{s1} and T_{s2}. This phenomenon can be explained by heat transfer equation number 18, which is provided below. Therefore, it is apparent that as one moves along the cold plate, the surface temperature rises due to the increasing temperature of the working fluid and the application of heat flux.

$$T_s(x) = T_i + \frac{q''.P.x}{\dot{m}.C_p} \tag{18}$$

Where P indicates the cross-sectional primitive.

Table 4
Detailed surface temperature for $\dot{m}$= 1 *l/min* flow rate for all studied cases.

Studied Case	T_{s1}	T_{s2}	T_{s3}	T_{s4}	$T_{s,ave}$
Plain CP-500 W	91.6	91.4	96.6	96.8	94.2
Rectangular MCH CP-500 W	88.9	88.4	93.4	93.7	91.1
Arc shape MCH CP-500 W	88.3	88	92.7	93.1	90.5
Sin wave shape MCH CP-500 W	87.7	87.3	91.7	92.2	89.7
Plain CP-500 W + JI	90.5	90.2	95.4	95.8	93.0
Rectangular MCH CP-500 W + JI	86.9	87.1	90.5	90.8	88.9
Arc shape MCH CP-500 W + JI	86.4	86.8	89.5	89.8	88.1
Sin wave shape MCH CP-500 W + JI	84.5	84.8	88.3	88.6	86.5

Data availability

Data will be made available on request.

References

[1] L. Du, et al., Thermal-hydraulic analysis and geometric optimization on a microchannel with stacked combinations of ribs and cavities, Int. J. Therm. Sci. 208 (2025) 109456.
[2] M. Yang, B.-Y. Cao, Numerical study on flow and heat transfer of a hybrid microchannel cooling scheme using manifold arrangement and secondary channels, Appl. Therm. Eng. 159 (2019) 113896.
[3] A. Ruichek, et al., Immersion cooling fluid comparison using a single-phase immersion/liquid technique for data centers, Appl. Therm. Eng. 280 (2025) 128355.
[4] R. Kandasamy, J.Y. Ho, P. Liu, T.N. Wong, K.C. Toh, S.J. Chua, Two-phase spray cooling for high ambient temperature data centers: evaluation of system performance, Appl. Energy 305 (2022) 117816.
[5] N. Wang, B. Tian, Y. Guo, J. Li, S. Shao, Investigation on liquid-cooled heat sink integrating topology optimization and microchannel design for high heat flux chip cooling, Appl. Therm. Eng. 281 (2025) 128740.
[6] S.K. Samal, H.-C. Chang, Y. Fulpagare, C.-C. Wang, Thermal management of data centers: Chip-scale cooling using novel distributed inlet–outlet jet impingement liquid cold plate, Appl. Therm. Eng. 271 (2025) 126360.
[7] B. Ramakrishnan, et al., Experimental characterization of two-phase cold plates intended for high-density data center servers using a dielectric fluid, J. Electron. Packag. 143 (2) (2021) 020904.
[8] M. Yang, M.-T. Li, Y.-C. Hua, W. Wang, B.-Y. Cao, Experimental study on single-phase hybrid microchannel cooling using HFE-7100 for liquid-cooled chips, Int. J. Heat Mass Transf. 160 (2020) 120230.
[9] J. Hu, C. Chen, X. Wang, G. Xin, M. Wang, Improvement of flow and heat transfer performance of microchannels with different ribs using topology optimization, Appl. Therm. Eng. 244 (2024) 122672.
[10] G. Zhai, et al., Numerical analysis on thermal and flow performance of honeycomb-structured microchannel cooling plate for IGBT, Energies 18 (16) (2025) 4455.
[11] L. Du, W. Hu, N. Deng, Z. Zhang, H. Wang, Computational analysis of heat transfer and fluid flow characteristics in a diamond microchannel heat sink with orthogonal ribs, Case Stud. Therm. Eng. 67 (2025) 105850.
[12] Z.-X. Wang, W.-Q. Tao, Heat transfer and pressure drop characteristics of microchannel cold plate in commercial CPU-package cooling system, Int. J. Heat Mass Transf. 246 (2025) 127060.
[13] J. Elliott, A. Robinson, Optimisation of liquid jet impingement coldplate for an overclocked CPU with multiple discrete cores, Therm. Sci. Eng. Prog. 67 (2025) 104221.
[14] Q. Sun, J. Guo, S. Zhou, M. Chen, D. Geng, R. Tao, Synergistic design of bi-level heat sink combining topology-optimized microchannels with jet impingement for high-heat-flux applications, Int. J. Heat Mass Transf. 255 (2026) 127875.
[15] M. Peng, L. Chen, W. Ji, W. Tao, Numerical study on flow and heat transfer in a multi-jet microchannel heat sink, Int. J. Heat Mass Transf. 157 (2020) 119982.
[16] M. Zunaid, A. Husain, B.S. Chauhan, R. Sahu, Numerical analysis of inclined jet impingement heat transfer in microchannel, Mater. Today Proc. 43 (2021) 557–563.
[17] W. Gao, J.-F. Zhang, Z. Qu, W. Tao, Numerical investigations of heat transfer in hybrid microchannel heat sink with multi-jet impinging and trapezoidal fins, Int. J. Therm. Sci. 164 (2021) 106902.
[18] Z. Tian, Z. Huang, S. Xu, K. Li, W. Gao, Direct liquid cooling heat transfer in microchannel: experimental results and correlations assessment, Appl. Therm. Eng. 223 (2023) 120020.
[19] S. Wu, K. Zhang, G. Song, J. Zhu, B. Yao, Experimental study on the performance of a tree-shaped mini-channel liquid cooling heat sink, Case Stud. Therm. Eng. 30 (2022) 101780.
[20] J. Miao, C. Li, M. Pan, Experimental and numerical analysis of variable cross-section channel liquid cooling plate for server chips thermal management, Therm. Sci. Eng. Prog. 49 (2024) 102470.
[21] M. Shanmugam, L.S. Maganti, Experimental investigation of microchannel heat sink performance under non-uniform heat load conditions with different flow configurations, Int. J. Therm. Sci. 203 (2024) 109128.
[22] T. Adibi, N.M. Maleki, E. Tavousi, A. Keshmiri, Enhancing the heat transfer efficiency in heated tube with a novel multi-twisted blade Turbulators: a numerical analysis, Int. Commun. Heat Mass Transf. 169 (2025) 109717, https://doi.org/10.1016/j.icheatmasstransfer.2025.109717.
[23] M.I. Afridi, et al., Enhancing the thermal performance of microchannel cold plates via controlled bubble injection for next-generation high-power electronic chips, Int. Commun. Heat Mass Transf. 172 (2026) 110621.
[24] R. Xiao, P. Zhang, L. Chen, Y. Zhang, Y. Hou, Experimental study on cooling performance of a hybrid microchannel and jet impingement heat sink, Appl. Sci. 12 (24) (2022) 13033.
[25] T. Brunschwiler, B. Smith, E. Ruetsche, B. Michel, Toward zero-emission data centers through direct reuse of thermal energy, IBM J. Res. Dev. 53 (3) (2009) 11.